LAL 92-28
May 1992

Laboratoire de l'Accélérateur Linéaire

ACCELERATION OF POLARIZED PARTICLES

Jean Buon

To be published in "Advances of Accelerator Physics and Technologies" edited by Prof. H. Schopper (World Scientific Publishing Co)

U.E.R
de
l'Université Paris-Sud

Institut National
de Physique Nucléaire
et
de Physique des Particules

Bâtiment 200 - 91405 ORSAY Cedex

LAL 92-28
May 1992

ACCELERATION OF POLARIZED PARTICLES

J. BUON
Laboratoire de l'Accélérateur Linéaire, IN2P3-CNRS
et Université de Paris-Sud, F-91405 Orsay Cedex , France

ABSTRACT

The spin kinetics of polarized beams in circular accelerators is reviewed in the case of spin-1/2 particles (electrons and protons) with emphasis on the depolarization phenomena. The acceleration of polarized proton beams in synchrotrons is described together with the cures applied to reduce depolarization, including the use of "Siberian Snakes". The in-situ polarization of electrons in storage rings due to synchrotron radiation is studied as well as depolarization in presence of ring imperfections. The applications of electron polarization to accurately calibrate the rings in energy and to use polarized beams in colliding-beam experiments are reviewed.

1. Introduction

The last two decades have seen the development of techniques to accelerate polarized beams at high energy. They provide a new tool for research in physics, allowing to discriminate the contributions of different spin states in the interaction between particles. The cross-section of a reaction is ultimately measured by bombarding a polarized target with a polarized beam.

Polarized protons have been successfully accelerated in several synchrotrons. At Saturne[1,2] (Saclay) beams of 2×10^{11} proton/burst, fully polarized, are routinely accelerated at energies up to 3 GeV. The maximum energy of 22 GeV has been reached at the AGS[3] (Brookhaven). Polarized electron beams have also been accelerated at the Bonn 2.5 GeV synchrotron[4], at the high-energy linac of SLAC to 22 GeV[5] and recently up to 46 GeV at the Stanford Linear Collider (SLC)[6]. However, the most outstanding observation is the in-situ polarization build-up of electron beams circulating in storage rings up to the highest energy of 46 GeV at LEP[7].

The main difficulty to obtain polarized beams at high energy is to reduce the depolarizing effects when particles circulate in a synchrotron or a storage ring and that become larger and larger when their energy increases. For that reason the aim is here to describe the physics of spin motion in a circular accelerator, the depolarizing mechanisms that drive dangerous spin resonances and the cures that are applied to reduce them (see also previous reviews[8,9]). One of the most promising techniques is the implementation of "Siberian Snakes"[10,11] that have been shown[12,13] to suppress depolarization of a proton beam during acceleration at least at moderate energies. Nevertheless, the acceleration of polarized beams at the highest energies ($\geq$ 100 GeV) is a challenge that would likely need an extreme tuning of the accelerators.

Here there is no attempt to study in detail all aspects of spin behavior in circular accelerators. The purpose is just to introduce the physical concepts and to briefly describe the depolarizing mechanisms of electrons and protons, the in-situ polarization of the electrons, as well as the applied cures and the recent achievements. The polarized sources and the polarimeters are beyond the scope of this article.

To begin with, the meaning of polarization for a spin-1/2 particle beam is reminded in Section 2. The spin motion in static fields is discussed in Section 3. In Section 4. the concept of spin-orbit coupling is introduced as the basis of the depolarizing effects that occur on spin resonances. The mechanism of depolarization on spin resonances is studied in Section 5 and the different kinds of spin resonances arising in circular accelerators are given .

The acceleration of polarized protons in synchrotrons is reviewed in Section 6 (see also previous reviews[14,15,16]). The depolarization due to resonance crossing during acceleration and the cures applied is discussed in Section 7. The principle of a "Siberian Snake" to overcome depolarization on spin resonance crossing and the first experimental confirmation are reviewed in Section 8.

In the last part the particular case of relativistic electron beams in storage rings is considered (see also previous reviews[17,18,19]). The in-situ polarizing mechanism due to synchrotron radiation (the Sokolov-Ternov effect[20]) is introduced in Section 9. In presence of ring imperfections the synchrotron radiation is also responsible for a harmful spin diffusion. That depolarizing mechanism, enhanced on spin resonances, is discussed in Section 10 as well as ways to improve polarization. The method to accurately calibrate an electron ring in energy, by crossing a RF resonance applied on purpose, is studied in Section 11. Finally, the requirements to perform electron-positron and electron-proton experiments with polarized electron beams in storage rings are reviewed in Section 12.

2. Polarization of a spin-1/2 particle beam[21]

With respect to an arbitrary quantification axis Oz, a spin-1/2 particle (electron, muon, proton,...) has two spin eigenstates labelled $S_z = +\hbar/2$ ("up" state) and $S_z = -\hbar/2$ ("down" state) respectively. The corresponding magnetic moment along that axis is:

$$\mu_z = g \frac{e}{2m_0} S_z \qquad (1)$$

where e and m_0 are the electric charge and the rest mass of the particle respectively (μ_Z has same sign than S_z for a proton, and opposite sign for an electron according to the sign of their electric charge). The gyromagnetic ratio g is 2 for a point-like spin-1/2 particle in the Dirac theory. For real particles its deviation from 2 is measured by the gyromagnetic anomaly[22] a = (g − 2)/2 (very often designated by G in the literature):

electron	muon	proton
$a = 1.15965\times10^{-3}$	1.16592×10^{-3}	1.79285

Moreover, a charged particle at rest, placed in a field of magnetic induction B parallel to Oz, has a magnetic energy W given by:

$$W = -\mu_z B \tag{2}$$

The polarization of a beam with N spin-1/2 particles is characterized by a direction along which one observes N_+ particles with spin "up" and N_- particles with spin "down" ($N = N_+ + N_-$). The degree of polarization is:

$$P = \frac{N_+ - N_-}{N_+ + N_-} \tag{3}$$

A beam is unpolarized ($P = 0$) when $N_+ = N_-$ and fully polarized when either N_+ or N_- vanishes ($P = \pm 1$). Finally, the beam polarization is represented by a vector **P** lying along the direction of polarization with a length equal to the degree of polarization. The vector **P** is in fact the statistical average of the spin quantum operator **S** over all the particles in the beam. Therefore, according to the general rules of quantum mechanics, the polarization vector behaves as a classical quantity. Its evolution can be described by a deterministic and classical equation that takes account for its motion in a static electromagnetic field, as well as quantum spin flips between the eigenstates due to interaction with a radiative field.

That description of beam polarization can be extended to the case of a deuteron beam. Deuterons are particles of spin one with three eigenstates: $S_z = +\hbar, 0, -\hbar$. Their gyromagnetic anomaly[23] is $g = -0.142562$. The polarization vector **P** is again the statistical average of the spin quantum operator **S** and is mostly sufficient to determine the polarization state. One can incorporate the case of polarized deuteron beams in the description given here. Their acceleration is similar to the acceleration of a proton beam and even easier.

Hereafter, one considers a test particle as a representative of an ensemble of particles with same trajectory and same energy. Its spin vector **S** is intended to be the statistical average of the spin operator on that ensemble, i.e. the polarization vector of that ensemble. It must not be confused with the quantum spin operator itself. The spin vector **S** leads to a semiclassical description of spin dynamics. The overall polarization vector **P** of the beam is obtained by averaging **S** over all the possible trajectories and energies in the beam.

3. Spin precession in a static electromagnetic field

For protons the motion of the spin vector **S** in a static field is a pure precession. For electrons at relativistic energies there are also radiative effects. Although they are important (accounting for the Sokolov-Ternov polarizing effect[20] and spin diffusion), they can in general be considered as discrete quantum jumps between which the motion is a pure precession as for protons. It is natural to study the precession first, as it leads to a spin-orbit coupling that is the reason of all the depolarization phenomena.

For non-relativistic particles, the spin precession results from the conservation of the magnetic energy given by the Eq. 2. The spin vector **S** rotates about the magnetic induction **B** at the Larmor frequency:

$$\Omega_L = g \frac{eB}{2m_0} \tag{4}$$

For point-like spin-1/2 particles ($g = 2$) the spin precession frequency is equal to the cyclotron frequency:

$$\Omega_c = \frac{eB}{m_0} \tag{5}$$

with which the particle velocity rotates about the magnetic field. The relative deviation of the spin precession frequency is just the gyromagnetic anomaly a:

$$\frac{\Omega_L - \Omega_c}{\Omega_c} = a \tag{6}$$

The measurement of that deviation is the principle of all the "g–2" experiments that aim to measure the gyromagnetic anomaly.

At relativistic energies the spin motion in a static electromagnetic field is given by the Bargman-Michel-Telegdi equation[24] (abbr. BMT equation):

$$\frac{d\mathbf{S}}{dt} = \Omega_{BMT} \times \mathbf{S} \tag{7}$$

with:

$$\Omega_{BMT} = -\frac{e}{m_0 \gamma}\left[(1 + \gamma a)\,\mathbf{B}_\perp + (1 + a)\,\mathbf{B}_{//} - \left(a + \frac{1}{\gamma + 1}\right)\gamma\boldsymbol{\beta} \times \frac{\mathbf{E}}{c}\right] \tag{8}$$

where $\mathbf{B}_\perp$ ($\mathbf{B}_{//}$) is the transverse (longitudinal) component of the induction **B** relative to the particle velocity; γ is the relativistic Lorentz factor and $\boldsymbol{\beta}$ is the velocity vector in units of the light velocity c (all quantities in MKS units). In that equation the fields **E** and **B**, and the time t, are expressed in the laboratory frame. On the other hand, the spin vector **S** is expressed in the

instantaneous rest frame of the particle and the BMT equation includes the Thomas precession[25,26] that occurs in that frame.

The spin precession has the following general properties:

i) The rotating strength of an electric field E is of the same order of magnitude as a magnetic field B = E/*c*. An electric field of 3×10^8 V/m has a rotating strength comparable to that of a one-Tesla magnetic field. Applied electric fields in accelerators have much smaller amplitude. Their effect on the spin is negligible. However, in the space charge fields of an ultra-relativistic beam the ratio of the electric field to the magnetic field becomes equal to c. It is well-known that the electric and magnetic forces between two charged and ultra-relativistic particles cancel out when their velocities are parallel. On the other hand they are equal and add to each other when their velocities are anti-parallel. For the spin precession the same property results from the BMT equation. At ultra-relativistic energies one can neglect space charge fields, apart in the beam-beam interaction of colliding beams.

ii) The spin rotating strength of a field $\mathbf{B}_{//}$ parallel to the velocity is inversely proportional to the particle momentum **P**, as the velocity rotating strength of a transverse field $\mathbf{B}_{\perp}$ is. The parallel-field integral $\int B_{//} ds$, needed to rotate the spin by one radian is:

$$\int B_{//}\, ds\ (Tm/rad) = \frac{10.479}{\pi} \times \frac{P(GeV/c)}{1+a} \tag{9}$$

At 1 GeV/c, a parallel-field integral of 10.479 Tm is needed to rotate the spin by 180° for a particle with vanishing gyromagnetic anomaly.

iii) The difference in frequency of spin and velocity precessions about a transverse magnetic field $\mathbf{B}_{\perp}$:

$$\Omega_a = \Omega_{BMT} - \Omega_c = \gamma a \left[-\frac{e}{m_0 \gamma} \mathbf{B}_{\perp} \right] \tag{10}$$

is exactly independent of the particle energy, and is γa times larger than the relativistic cyclotron frequency $\Omega_c = eB_{\perp}/m_0\gamma$:

$$\Omega_a = \gamma a\ \Omega_c \tag{11}$$

The vector Ω_a is the spin rotation vector with respect to a frame attached to the particle trajectory (named orbit frame) since this frame rotates at the cyclotron frequency Ω_c as the velocity rotates.

The transverse-field integral $\int B_{\perp} ds$, required to rotate the spin by one radian w. r. t. the orbit frame, is for a proton:

$$\int B_{\perp}\, ds\ (Tm/rad) = \frac{5.484}{\pi} \times \frac{Pc}{E} \tag{12}$$

and for an electron:

$$\int B_{\perp}\, ds\ (Tm/rad) = \frac{4.618}{\pi} \times \frac{Pc}{E} \tag{13}$$

where E is the total relativistic energy of the particle. In a given transverse field, a proton and an electron with the same velocity have comparable spin rotation, as the larger mass of the proton is compensated by its larger gyromagnetic anomaly.

iv) At high energies, when $\gamma a >> 1$, the spin rotating strength of a parallel field becomes much weaker than the strength of a transverse field. Transverse fields are more economical for spin manipulations at high energies. Moreover, the precession frequency Ω_{BMT} in a transverse field becomes nearly energy-independent and spin rotation requires much less bending field than the trajectory does. In other words the spin vector precesses much faster than the particle velocity.

v) In a ring one can consider the one-turn mapping attached to a particle circulating on the reference orbit at the reference energy. It is made of successive rotations in the magnetic elements, resulting in an overall one-turn spin rotation. In general the precession axis $\mathbf{n}(s)$ of that rotation depends on the position s of the initial point along that orbit. It can be shown[9,27] that $\mathbf{n}(s)$ is a solution of the spin motion. That solution is also a closed solution as that precession axis is invariant under the one-turn spin rotation. For instance the spin closed solution is vertical in an ideal ring lying in a horizontal plane. Usually horizontal bending fields are small and the spin closed solution is nearly vertical.

Now, any other spin direction precesses about $\mathbf{n}$ and the precession angle Ψ of the one-turn mapping attached to the reference orbit defines the spin tune $\nu = \Psi/2\pi$. Similarly to the betatron and synchrotron tunes, the spin tune gives the number of 2π precessions per turn. According to the Formula 11, the spin tune for an ideally planar ring, in the orbit frame, is given by:

$$\nu = \gamma a \tag{14}$$

i.e. numerically by:

$$\nu = \begin{array}{ccc} \text{electrons} & \text{protons} & \text{deuterons} \\ \dfrac{E(GeV)}{0.44065} & \dfrac{E(GeV)}{0.52335} & \dfrac{E(GeV)}{13.1565} \end{array} \tag{15}$$

as function of the total relativistic energy E. The spin tune increases linearly with the energy. Electrons and protons of same energy have comparable spin tunes. In real rings with small vertical bends the spin tune cannot deviate very much from that value. On the contrary a "Siberian Snake"[10,11] is a magnetic device with strong vertical bends such that the spin tune becomes equal to 1/2 independently of the energy.

4. Spin-orbit coupling

According to the BMT equation (Formula 7), the spin precession of a particular particle in a beam depends on its energy and on the fields encountered along its trajectory. Particles with different either energies or trajectories have different spin motion. The spin precession is coupled to the orbital motion.

For instance, in an ideally planar and horizontal ring, the magnetic field stays vertical and transverse along a horizontal trajectory. On the other hand, along a trajectory with a vertical betatron oscillation, the field is horizontal and proportional to the vertical displacement in the quadrupoles (see Fig.1). A small parallel field is also experienced in the horizontally bending magnets where the trajectory has a vertical slope. Along these two trajectories, the fields are different and the spin precession too. In particular the horizontal field B_x bends the spin away from the vertical direction.

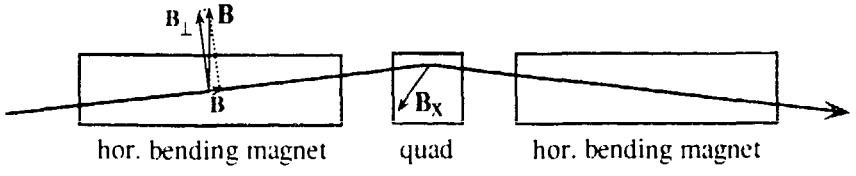

Figure 1: Fields along a trajectory oscillating in the vertical plane and passing through horizontally bending magnets and quadrupoles.

In general the spin-orbit coupling is responsible for beam depolarization. The spread of energies and trajectories among the particles in a beam leads to a spread in the spin precession. Assuming that all the individual spins would initially point to the same direction (full polarization), after some time they will spread in different directions. The length of the beam polarization vector, i.e. the degree of polarization, must decrease. However, the spin-orbit coupling is not a sufficient condition to observe a significant depolarization. There must also be a constructive pile-up of all the bends given to the spins in the magnets. That explains why depolarization occurs only on spin resonances where these bends fulfill a stationary condition of phase.

In the ideal case of a beam with vanishing vertical emittance and circulating in an exactly planar ring, the particles undergo horizontal oscillations and experience vertical fields only. Assuming a vertical polarization of the beam, the spins are not bent by these fields and there is no depolarization. In practical cases one tries to correct as much as possible the ring defects to limit the depolarization of a vertically polarized beam. In particular the first condition to maintain the polarization is to have a very good closed orbit.

In general when the sum of all the bends given to the spins along the ring circumference cancels out, the ring is said[28] to be "spin-transparent". That condition is fulfilled in the previous ideal case. Depolarization is minimized by making the ring more spin-transparent. The spin matching consists to apply special correction schemes to improve spin transparency. Moreover

in a planar ring the defects bend the spin closed solution **n** away from the vertical. The spin matching has also the effect of making **n** more vertical.

The reverse of the spin-orbit coupling is expected. Different spin states must lead to slightly different trajectories as observed in experiments of the Stern-Gerlach type. However, that reverse coupling is very weak at high energies. The magnetic energy of a spin state is only of the order of $ae\hbar/2m \approx 10^{-10}$ MeV/Tesla, much smaller than the kinetic energy.

5. Spin resonances

In a real ring that is not spin-transparent an oscillating particle and the reference particle (circulating on the reference orbit) experience different fields. Their difference is a perturbing magnetic field **b**(s). It bends the spin vector **S** of the oscillating particle away from the spin closed solution **n**(s) attached to the reference particle. Only the component $\mathbf{b}_\perp$ perpendicular to the spin closed solution **n** needs to be considered. That bending varies in direction (perpendicular to **n**) and amplitude, following the variation of the particle oscillation along the longitudinal position s. That perturbation of the spin **S** motion is coupled with its normal precession about **n** and results in a spiraling motion on a spin resonance (see Fig.2).

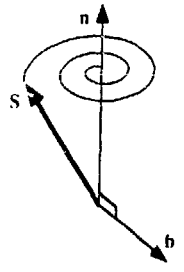

Figure 2: On a spin resonance the spiraling motion of a spin vector **S** that precesses about **n** and that is bent away from the spin closed solution **n**(s) by a perturbing magnetic field **b**(s).

The simplest example to understand how depolarization occurs on a spin resonance is the case of an isolated resonance. It is driven by a perturbing field **b**(s) that simply rotates about the spin closed solution **n**(s) at a frequency ν_r (in units of the revolution frequency Ω_c). If that frequency significantly differs from the spin precession frequency ν (assumed to be uniform), the phase difference between the motions of **S** and of **b** linearly increases with time. All the successive kicks on a spin vector **S** point to different directions and average to zero in a finite time. In spite of the perturbing field there is no significant depolarization. On the contrary, when ν_r and ν coincide, the phase difference between the motions of **S** and of **b** is stationary and the kicks add up constructively (see Fig. 3). In addition to its precession about **n**, the spin vector is rotating about **b** at the frequency:

$$\varepsilon = (1+\gamma a)\frac{b}{B_0} \qquad (16)$$

in units of the revolution frequency Ω_c, assuming that **b** is transverse and B_0 being the field of the normal bending magnets. The combination of these two rotations give the spiraling motion of the spin vector.

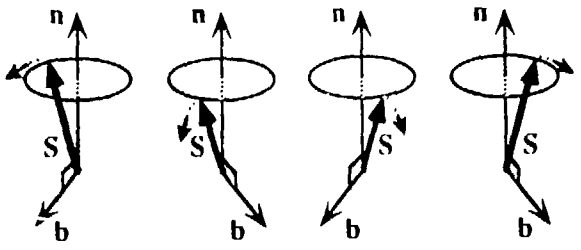

Figure 3: The directions of a spin vector **S** and of the perturbing field **b** at different times on a spin resonance. The dashed arrows show the directions of the kicks given to **S** that all bend it away from **n**.

The rotation about **b** periodically exchanges the two spin states "up" and "down". Such a spin resonance is exactly what happens in a Nuclear Magnetic Resonance experiment. The polarized beam is the analogue of a substance with spin-aligned nuclei. The perturbing field plays the role of the applied RF field in a NMR experiment.

Now, considering that the perturbing field **b** varies in amplitude and in rotation phase for different particles, their spin vectors **S** rotate in different directions with different frequencies. They will rapidly point to different directions and the beam is depolarized.

The frequency ε, given by the Formula 16., measures the speed with which the spin vector is bent away from the direction of **n**. It is the strength of the resonance. It also measures the width of the resonance, as the bending of **S** is negligible when the frequency difference $\nu - \nu_r$ of **b** and **S** becomes larger than ε.

In practical cases the perturbing field **b** results from the betatron and synchrotron oscillations of the particles. The Fourier spectrum of its motion is made of lines that are linear combinations of the betatron and synchrotron frequencies and of the revolution frequency. On the other hand, the Fourier spectrum of the spin precession is made of a main line at the spin precession frequency with satellites separated by the revolution frequency. Every pair of lines, one of the **b**-spectrum and one of the precession spectrum, drives one spin resonance. The general formula giving the spin tunes of the resonances in terms of the betatron and synchrotron tunes is:

$$\nu = k + k_x Q_x + k_z Q_z + k_s Q_s \qquad (17)$$

where k, k_x, k_z and k_s are all integers. One distinguishes the horizontal (vertical) betatron resonances: $\nu = k \pm Q_{x,z}$, driven by linear betatron oscillations and the synchrotron resonances: $\nu = k \pm Q_s$, driven by linear synchrotron oscillations. Normally the integer k is a multiple of the accelerator superperiodicity p. However the defects generally break the superperiodicity and weaker spin resonances occur for k-values not multiple of p. Moreover, large-amplitude particle oscillations drive non-linear spin resonances that correspond to: $|k_x| + |k_z| + |k_s| > 1$. All kinds

of spin resonances are repeated when the spin tune increases by one unit, i.e. every 523 Mev for protons and every 440 Mev for electrons.

6. Acceleration of polarized protons in synchrotrons

Polarized protons have been successfully accelerated at high energies (larger than one GeV) in several synchrotrons: Saturne[1,2] at Saclay (up to 3 GeV), the KEK PS[29] at Tsukuba (up to 7 GeV), the ZGS[30] at Argonne (up to 12 GeV) and the AGS[3] at Brookhaven (up to 22 GeV). The most successful one is Saturne where proton, and also deuteron, polarized beams are routinely accelerated and used by the physicists. The highest energy (22 GeV) has been reached at the AGS and seems to be the limit of the present technology beyond which new provisions are needed to counteract large depolarization by numerous and strong spin resonances. One way is to use "Siberian Snakes" that, in an experiment[12,13] at the Indiana University Cyclotron Facility (IUCF) Cooler Ring, have been shown efficient to suppress depolarization on spin resonances.

At Saturne[1,2] 2.10^{11} particles per burst, either protons or deuterons, delivered by a polarized source with 90% polarization, are first injected and accelerated in the Mimas booster up to 47 MeV. Then they are extracted and injected in the Saturne main ring where they are accelerated up to the top energy. At injection in the rings the beam polarization is vertical. During acceleration the spin tune increases with the energy linearly (see Formula 14). Spin resonances are crossed when the spin tune takes one of the values given by the Formula 17. In the booster the vertical betatron tune Q_z must be set at a high value (2.48) to avoid the intrinsic resonance $\nu = 4 - Q_z$ even in presence of a large tune shift due to space charge effect at injection. In the main ring, depending on the extraction energy, at most 15 resonances are crossed (see Fig. 4).

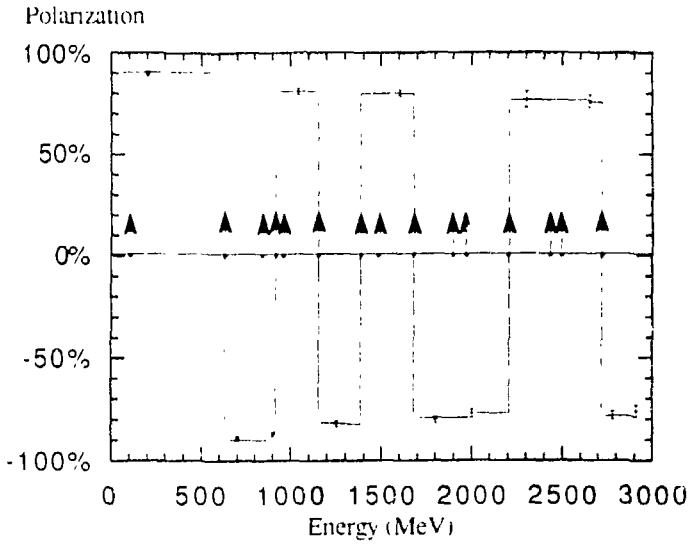

Figure 4: The vertical polarization as function of the proton energy during the acceleration cycle in Saturne[1,2]. The points with error bars are the experimental data. The arrows show the locations of the spin resonances. The solid line is a hand-drawn line showing the spin flips at the crossings of seven resonances.

Special provisions are made to avoid depolarization at the resonance crossings, as described below. The net effect is only a spin reversal for some of these resonances. At the maximum energy of 3 GeV the overall depolarization during the complete cycle of acceleration is less than 15% as measured by a high-energy polarimeter.

At the AGS[3] a polarized source has been used to deliver a 25 μA H^- beam with 75% polarization. That beam was first accelerated in a RFQ, then in a linac up to 200 MeV (see Fig.5). After electron stripping through a thin carbon foil, the polarized proton beam was injected in the main ring. At the maximum energy of 22 GeV the proton beam ($\simeq 2 \times 10^{10}$ ppp) has been extracted and transported to the experimental area to bombard a polarized proton target.

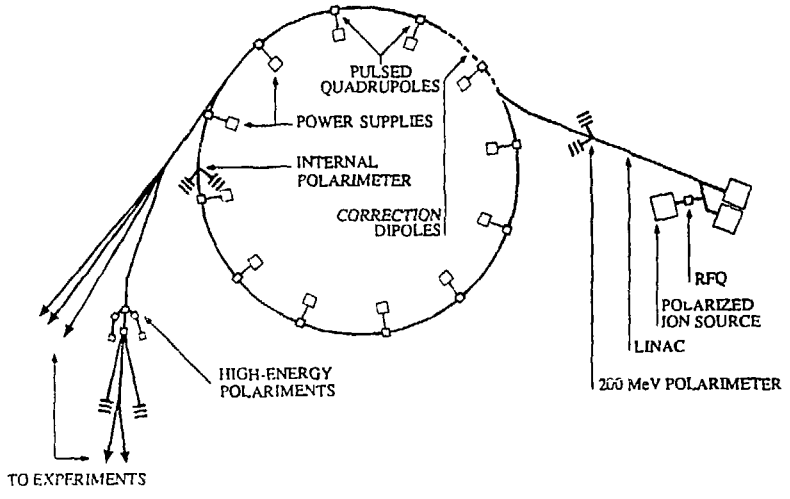

Figure 5: The AGS[3] lay-out for the acceleration of polarized protons.

The polarization is measured by polarimeters at several stages of the acceleration process: downstream of the linac before injection in the ring, inside the ring, and after extraction. During the acceleration cycle one had to overcome 45 strong spin resonances to maintain the polarization up to 22 GeV, making the commissioning of the proton polarized beam a painstaking effort. The depolarization on the resonances is minimized using 95 dipole correctors and 12 pulsed quadrupoles. The obtained maximum polarization was 45% above 16 GeV/c proton momentum (see Fig.6).

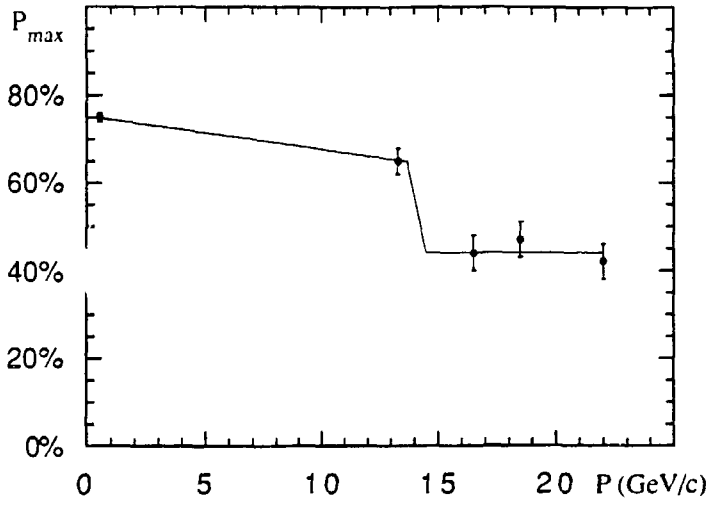

Figure 6: The maximum AGS beam polarization[3] as function of the beam momentum. The solid line shows the sharp polarization loss near 14 GeV/c.

7. Depolarization by resonance crossing in proton synchrotrons

As the beam polarization must be maintained vertical to approach spin transparency, only the projection P_z of the polarization vector along the vertical line is considered. Any depolarization is measured as a decrease of the vertical projection. The main spin resonances responsible for the most important vertical depolarization are of two types:

i) The vertical betatron resonances, named intrinsic resonances, at spin tune values:

$$\nu = kp \pm Q_z \tag{18}$$

where p is the superperiodicity of the ring assumed to be perfect and k is any integer. They are driven by the vertical betatron oscillations of the particles. The horizontal magnetic fields along the oscillating trajectories bend the spin vectors away from the vertical line. That perturbing fields are encountered in the quadrupole lenses and in the combined-function magnets. When taking account of the ring imperfections, the superperiodicity is broken by the defects. New resonances appear where kp becomes

any integer. However, the not-superperiodic resonances driven by the imperfections are weaker than the intrinsic ones.

ii) The synchrotron resonances, named imperfection resonances, at spin tune values:

$$\nu = k \pm Q_s \tag{19}$$

They are driven by the horizontal and vertical synchrotron oscillations, together with vertical closed-orbit distortions due to imperfections. The closed spin solution **n** along the perturbed closed orbit is no more exactly vertical. Due to the horizontal and vertical dispersion (the latter also due to the defects), vertical and respectively horizontal perturbing fields are encountered along synchrotron trajectories. They bend the spin vectors away from the **n** direction. In most of the synchrotrons the synchrotron tune Q_s is much less than one. In the spectrum of spin resonances there are two synchrotron lines on both sides of each integer k. Usually these lines are not discriminated from the integer and these resonances are also named integer resonances. The most harmful imperfection resonances are those for which k = np±m where n is any integer and m is an integer close to Q_z.

For imperfection resonances the resonance strength ε scales linearly with the amplitude of the vertical closed-orbit and with the total proton energy (see Formula 16). It lies in the 10^{-3}-10^{-5} range at the AGS. For the intrinsic resonances that strength scales linearly with the energy and with the square root of the vertical emittance, lying in the 10^{-3} -10^{-2} range at the AGS.

During the acceleration cycle the spin tune ν increases monotonically and each resonance is crossed once. The width of the resonances, also measured by ε, is usually smaller than the resonance spacing. The resonances can be considered as if they would be isolated during crossing. The spin motion of an individual particle, when crossing a single resonance, can be simply studied by considering a rotating frame. It rotates about the spin closed solution **n**, nearly vertical in practice, at the same frequency ν_r than the perturbing field driving the resonance. With respect to that frame the perturbing field **b** is at rest. The spin vector **S** rotates about **n** at the frequency $\delta = \nu - \nu_r$ and about **b** at the frequency ε. Its overall rotation vector Ω has components δ along **n** and ε along **b** (see Fig.7). Far below the resonance δ is negative and much larger than ε; Ω is nearly antiparallel to **n**. When approaching the resonance, Ω starts to move into the direction of **b**. On top of the resonance Ω is exactly along **b**. Above the resonance Ω now moves into the direction of **n** and becomes nearly parallel to **n** far above the resonance. The resonance crossing leads to a complete reversal of the rotation vector Ω.

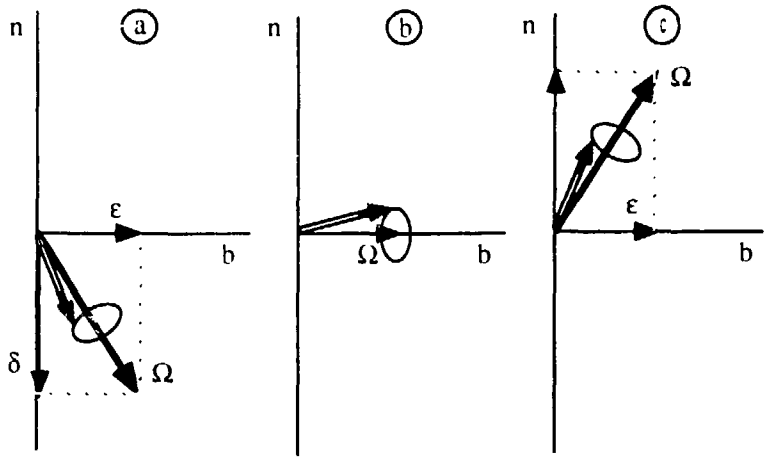

Figure 7: The spin rotation as seen in the rotating frame near an isolated resonance. The rotation vector is Ω with components ε along the driving field **b** and δ along the direction **n**:
a) below the resonance ($\delta < 0$),
b) on top of the resonance ($\delta = 0$),
c) above the resonance ($\delta > 0$).

The speed of the resonance crossing is measured by the rate α of the spin tune variation:

$$\nu = \nu_r + \alpha\theta \tag{20}$$

where θ is the azimuthal angle of the particle along the ring circumference. The "time" $\Delta\theta$ of the crossing is the width ε of the resonance divided by the rate α: $\Delta\theta = \varepsilon/\alpha$. During that time the rotation angle of the spin about **b** is: $\psi = \varepsilon\,\Delta\theta = \varepsilon^2/\alpha$. There are two extreme regimes of resonance crossing:

i) Fast crossing ($\psi << 1$): either the resonance is too narrow or the crossing rate is very large. There is not enough time to bend the spin vector away from the direction **n** and there is no depolarization.

i) Slow crossing ($\psi >> 1$): either the resonance is very broad or the crossing rate is very slow. The spin vector rotates much faster about the rotation vector Ω than the latter moves. The spin vector adiabatically follows the vector Ω in its motion and undergoes a complete reversal as Ω. After the crossing the vertical polarization has changed sign, but there is no depolarization.

Between these two extreme regimes of crossing there is a partial spin flip. The decrease of the vertical component S_z of the spin vector is quantitatively given by the Froissart-Stora Formula[31]:

$$\frac{S_z\,final}{S_z\,initial} = 2\,exp\left(-\frac{\pi\varepsilon^2}{2\alpha}\right) - 1 \tag{21}$$

that also includes the two extreme regimes of fast crossing and adiabatic spin flip (S_z final = ± S_z initial respectively). The width ε of a resonance depends on the oscillation amplitude of the considered particle. To obtain the decrease of the vertical beam polarization P_z, i.e. the depolarization, one must average the Froissart-Stora formula over the particles amplitudes.

The adiabatic spin flip has been observed at Saturne at the crossing of five imperfection resonances and of two intrinsic resonances. Figure 8 shows detailed measurements[32] of the vertical polarization showing the spin flip when the beam is slowly extracted in the vicinity of the imperfection resonance $\gamma a = 3$.

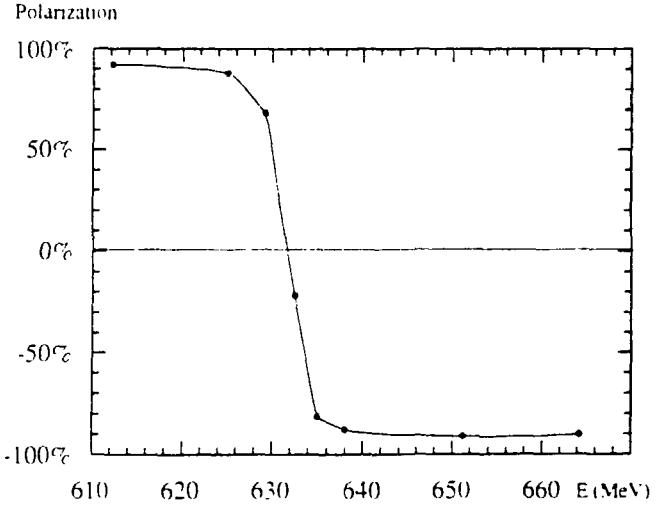

Figure 8: The vertical polarization P, as function of the total proton energy E, measured after slow extraction in the close vicinity of the imperfection resonance $\gamma a = 3$ at Saturne[32].

Two different methods have been applied to avoid depolarization at the crossing of resonances that are not enough strong to obtain a complete spin flip:

i) Compensation of the resonance strength ε (named also harmonic spin matching): with some dipole correctors one can control the harmonics of the vertical closed-orbit distortion that drive an imperfection resonance. After the usual closed-orbit correction one maximizes the polarization, measured with a polarimeter, by adjusting the dipole correctors. That method has been successfully applied[3] to compensate about 35 imperfection resonances at the AGS using 95 correctors (see Fig. 9).

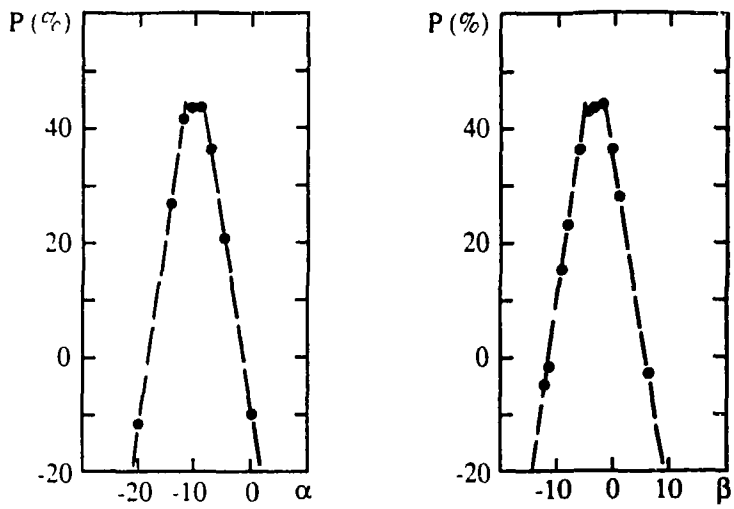

Figure 9: The vertical polarization as function of the amplitudes α and β of the sine and cosine (resp.) harmonics that compensates the strong imperfection resonance γa = 9 at the AGS[3].

The same method using dipole correctors is also applied at Saturne[1,2] to compensate the imperfection resonance γa = 2. Similarly some intrinsic resonances are compensated using quadrupolar correctors.

ii) Speed increase of resonance crossing (also named resonance jumping): when approaching an intrinsic resonance during acceleration, the vertical betatron tune is abruptly varied such that the resonance is crossed more rapidly (see Fig.10). Thereafter the initial tune is slowly restored. At the AGS 10 pulsed quadrupoles have been used to jump 7 intrinsic resonances. The betatron tune was lowered by 0.25 with a 1.6 μsec risetime and a 20 μsec falltime.

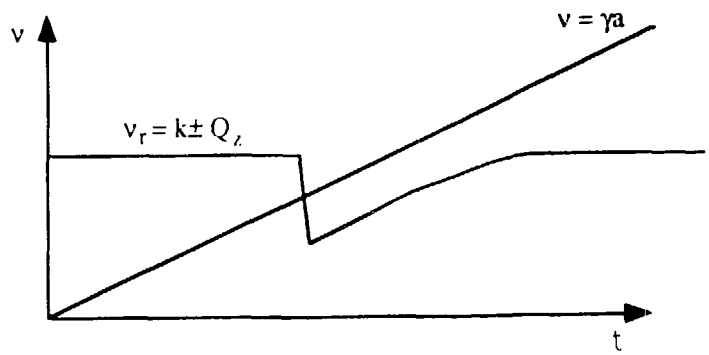

Figure 10: Variation with time of the spin tune ν and of the tune ν_r of an intrinsic resonance, when the vertical betatron tune Q_z is rapidly shifted.

8. Siberian Snakes

The number and the strength of the spin resonances, crossed during the acceleration cycle, increase with energy. To accelerate polarized protons at the AGS up to 22 GeV a considerable effort has been required to overcome depolarization with the preceding methods when crossing 45 strong spin resonances. That becomes unpractical at higher energies. Long time ago Ya. Derbenev and A. Kondatrenko[10,11] have proposed to equip rings with special magnet arrangements, after named "Siberian Snakes", that would avoid the crossing of all the resonances. With them the spin tune becomes equal to 1/2 and independent of energy. During acceleration the spin tune stays constant and never cross tune values of spin resonances.

In principle a Siberian Snake rotates any spin vector **S** by π about an axis **u** lying in the horizontal plane of the ring. In a ring equipped with one Siberian Snake, the spin closed solution **n**(s) lies in the horizontal plane, apart inside the magnets of the Siberian Snake. Figure 11. shows the motion of **n**(s) and of a spin vector **S**. At the point 0, opposite to the snake, **n**(0) is parallel to the axis **u**. Its direction **n**(πR) at the snake entrance is rotated into **n**'(πR) at the exit. The motion of **n**(s) before and after the snake are symmetric, such that **n**(s) again becomes parallel to the axis **u** after one turn. The motion of another spin vector **S** is also symmetric before and after passing through the snake. In particular at the point O its directions at the beginning and at the end of one turn are symmetric. Therefore they are connected by a π rotation about the axis **u** showing that the spin tune is effectively 1/2 (the spin tune is the rotation angle in units of 2π).

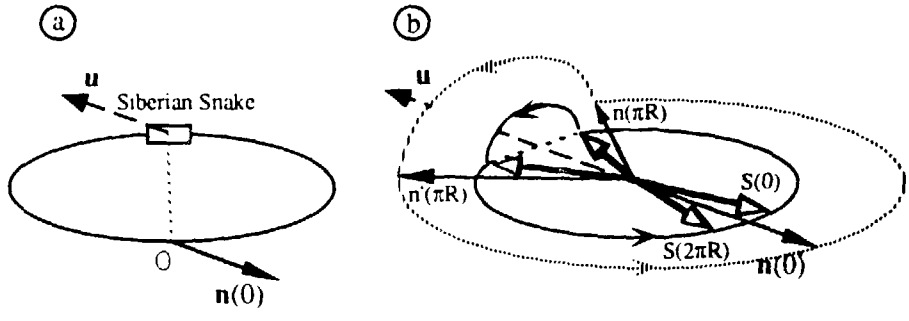

Figure 11: a) A ring equipped with a Siberian Snake located at s = πR. Its axis **u** lies in the horizontal plane. The spin closed solution **n**(0) is parallel to **u** at the origin O, opposite to the snake.
b) Horizontal precession of the spin closed solution **n**(s) and of a spin vector **S** lying in the ring plane. **n**(πR) and **n**'(πR) are the directions of **n**(s) at the entrance and at the exit of the snake respectively. S(0) and S(2πR) are the directions of the spin vector at the beginning and at the end of one turn respectively. The circles show the tracks of these vectors in the horizontal plane and about the Snake axis **u**.

The polarization behavior in a ring equipped with a snake is similar to the spin echo phenomenon used in NMR techniques. In a simple spin echo experiment a nuclear magnetic substance is magnetized and its magnetization vector **M** precesses about a stationary magnetic field $\mathbf{B}_0$ perpendicular to **M** (see Fig.12). Due to local field inhomogeneities, the magnetic moments μ of different nuclei precess at slightly different frequencies. If they were initially aligned in the same direction, they rapidly spread out and magnetization decreases. At time T a transient field is applied which rotates all the magnetic moments μ by π about the axis **u**. The fastest moments which were in advance before the time T become the latest after that π-rotation. At time 2T all the magnetic moments are again aligned together and the initial magnetization is restored. The spin vectors of the particles in a polarized beam are similar to the nuclear magnetic moments. They precess about the magnetic field of the ring bending magnets. The polarization vector **P** is the analogue of the magnetization **M**. The snake plays the role of the transient field and the spin-orbit coupling plays the role of the field inhomogeneities. The polarization decreases in the half turn preceding the snake and is restored at the end of the following half turn.

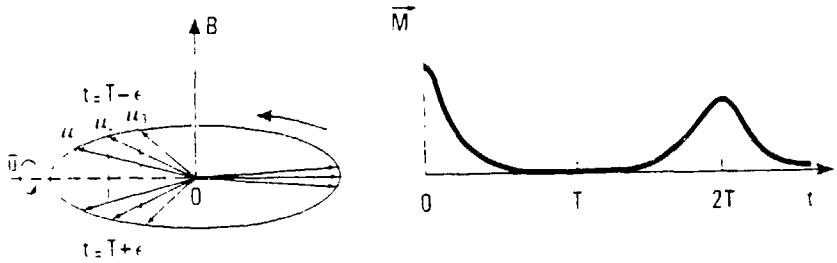

Figure 12: Scheme of a NMR spin echo experiment.
a) Precession of three magnetic moments $\mu_{1,2,3}$ about the magnetic field $\mathbf{B}_0$ with π-rotation at timeT (Positions at times T-ε and T+ε are shown).
b) The variation of the magnetization **M** with time t.

Generally one considers two kinds of Siberian Snakes[11,33]. A snake of type I rotates the spin by π about an axis parallel to the reference orbit. At low momentum P (Gev/c) it can be made of a single solenoid with a field integral of 3.752xP Tm (see Formula 9). A snake of type II rotates the spin by π about an axis perpendicular to the reference orbit. At high energies all kinds of snake should be made by sandwiches of several horizontally and vertically bending magnets.

The first experimental test[12,13] of a Siberian Snake to overcome depolarizing resonances has been done at the Indiana University Cyclotron Facility (IUCF) Cooler Ring. A type-I Siberian Snake, made of a superconductive solenoid and correcting quadrupoles, has been installed in the Cooler Ring. Other solenoids were used to produce a variable longitudinal field operating as a regulated defect driving imperfection resonances. Proton beams have been injected and stacked in the ring with either vertical or horizontal polarization to match the direction of the spin closed solution **n** (vertical when the snake is off and horizontal when the snake is on). An

internal polarimeter measured the vertical and radial components of the polarization. The Figure 13. shows the polarization data in the vicinity of the imperfection resonance $\gamma a = 2$ and the intrinsic resonance $\gamma a = -3 + \nu_z$. For the imperfection resonance the proton beam energy was fixed at 104 MeV (4 MeV below the top of the resonance) and the field integral of the imperfection solenoids was varied. With the snake off, the vertical polarization was consistent with zero apart when the defect field integral was nearly vanishing. On the contrary, with the snake on, the measured radial polarization was independent of the defect and close to its expected maximum. For the intrinsic resonance the proton beam energy was fixed to 177 MeV and the vertical betatron tune Q_z was varied. With the snake off, the vertical polarization was found to fall down to zero for tune values close to the resonance, while radial polarization was maintained at its maximum for all tune values when the snake was turned on. In another test the vertical tune was ramped in a way equivalent to acceleration through the intrinsic resonance. Without the snake the resonance crossing lead to 75% polarization loss and no observable depolarization with the snake turned on, proving the ability of Siberian Snakes to overcome depolarization during acceleration. That positive result opens the possibility to accelerate polarized proton beams at higher energies than the AGS.

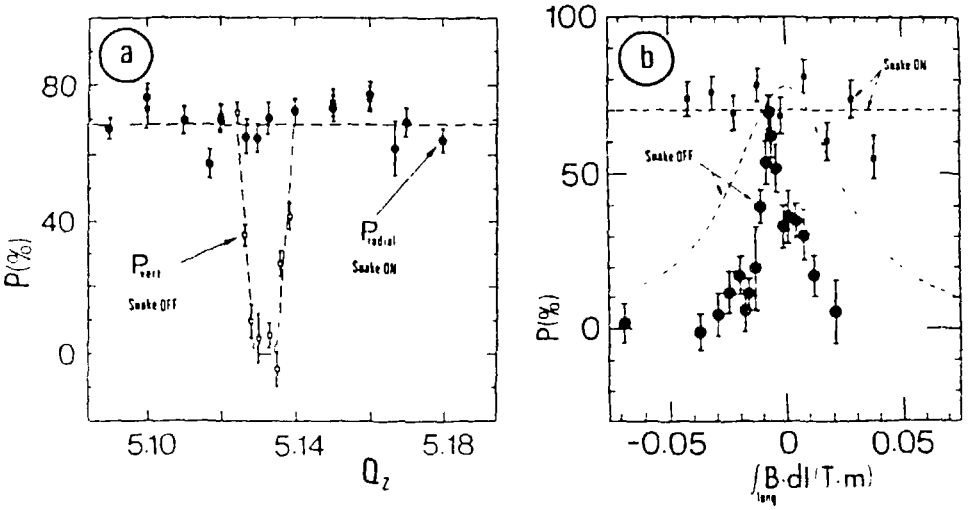

Figure 13: Polarization data at the IUCF Cooler Ring[12,13] with a Siberian Snake. The vertical and the radial polarizations are measured when the snake is respectively turned off and on:

a) At 177 MeV near the intrinsic resonance $\gamma a = -3+Q_z$, varying the vertical betatron tune Q_z.

b) At 104 MeV near the imperfection resonance $\gamma a = 2$, varying the field integral of the imperfection solenoids.

9. Polarization build-up of electrons in storage rings

The dynamics of electron and proton beams in high-energy storage rings are very different. The synchrotron radiation causes fluctuations and damping in electron oscillations. For instance, the emittance of a stored electron beam is only determined by synchrotron radiation. On the contrary, the emittance of a proton beam depends on its value at injection.

Similarly, the dynamics of polarization is different. A polarized source must be used to inject polarized protons and the final polarization is at most equal to its initial value. Electrons become transversely polarized in situ and do not need to be injected polarized. That is again due to synchrotron radiation which is the source of a polarizing process: the Sokolov-Ternov effect[20]. On the other hand, quantum fluctuations in synchrotron radiation also leads to depolarization. These two processes compete and lead to an equilibrium polarization.

The Sokolov-Ternov effect results from an asymmetry in synchrotron radiation. There are two possibilities when an electron emits a photon in a static magnetic field. Its spin state either does not change or is reversed (spin flip). Moreover, the probability of emission depends on the initial spin state. Measuring the spin state along the magnetic field, the rate of emission λ_+ with spin initially "up" is larger than the rate of emission λ_- with spin "down". In the case of spin flip the asymmetry A is very large:

$$A = \frac{\lambda_+ - \lambda_-}{\lambda_+ + \lambda_-} = \frac{8}{5\sqrt{3}} = 0.92376 \tag{22}$$

The "up" state flips to the "down" state much more often than the reverse. The "down" state gradually becomes more populated than the "up" state. The ultimate and maximum degree of polarization is equal to the asymmetry A, i.e. 92.4%. Finally, an electron beam polarization, antiparallel to the magnetic field, gradually increases from zero to its maximum. However, its rate is long compared to the synchrotron radiation rate due to the low probability of emission with spin flip. The characteristic time τ_p of polarization build-up is given by:

$$\tau_p^{-1} = \lambda_+ + \lambda_- = \frac{5\sqrt{3}}{8} c \lambda_c r_e \frac{\gamma^5}{\rho^3} \tag{23}$$

where r_e is the electron classical radius, λ_c is the Compton wavelength divided by 2π and ρ is the bending radius in the magnetic field. In a storage ring with a mean radius R, the theoretical polarization time is numerically given by:

$$\tau_p(sec) = 98.66 \frac{\rho^2(m)\, R(m)}{E^5(GeV)} \tag{24}$$

The polarization time decreases very rapidly when the energy is increased. It is due to the very fast increase of radiation rate that counteracts the low probability of spin flip in photon emission.

The polarization build-up by the Sokolov-Ternov effect has been observed in all the electron storage rings where it has been sought. The Table 1. gives polarization data for some of these rings.

Table 1: Polarization experimental data for some electron storage rings. The time τ_p is the theoretical polarization time given by Formula 24. at energy E. The polarization degree P is a typically measured value.

	VEPP[34]	VEPP2-M[35]	ACO[36,37]	BESSY[38]	SPEAR[39]	VEPP4[40]
E(GeV)	0.640	0.625	0.536	0.800	3.70	5.0
τ_p(min)	50	70	160	150	15	40
P(%)	52	90	90	>75	>70	80
	DORIS II[41]	CESR[42]	PETRA[43]	HERA[44]	TRISTAN[45]	LEP [6,46]
E(GeV)	5.0	4.7	16.5	26.7	29	46.5
τ_p(min)	4	300	18	40	2	300
P(%)	80	30*	80**	≈8	75**	15-20

Figure 14. shows the polarization build-up as function of time at 16.5 GeV in PETRA. The fifth power law of the polarization time versus energy is observed when the beam energy is changed in a storage ring. In particular the polarization time at LEP becomes very long in the lower part of its energy range: five hours at the energy (46 GeV) of the Z_0 vector boson production. The polarization time also increases as the third power of r, explaining why several rings have different polarization times at the same energy.

* after 120 min.

** after harmonic correction (harmonic spin matching).

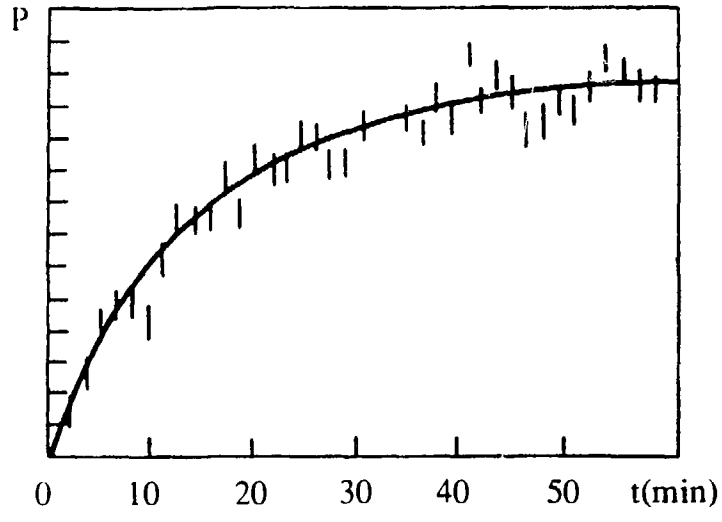

Figure 14: Polarization P (in arbitrary units) versus the time t in the storage ring PETRA at 16.5 GeV.

The experimental values (see Table 1.) indicate that the equilibrium polarization, without special corrections, is lower than the theoretical 92.4% value at multi-GeV rings. The polarization time is also lower than the theoretical value given by Formula 24. That results from the depolarization effect of synchrotron radiation as explained below.

A stored positron beam becomes polarized as well as an electron beam. However, the direction of polarization is opposite, i.e. parallel to the magnetic field. It is worth noting that in both cases the direction of polarization corresponds to a minimum of the magnetic energy (see Formula 2.). However, it has been shown that it is more a coincidence that a real cause[47].

In an ideally planar and at low energy, it has been shown[48] that the ultimate degree of polarization could even reach 99.2% due to the contribution arising from the electron recoil in the photon field. That would happen when the spin tune is in the vicinity of a vertical betatron spin resonance. However in real rings, with imperfections, depolarization on spin resonances dominate and polarization lower than 92.4% is always observed, particularly at high energies.

10. Depolarization by resonant spin diffusion in electron storage rings

In an electron storage ring the betatron and synchrotron oscillations are driven by the quantum fluctuations of synchrotron radiation. When a photon is emitted by an electron the sudden energy jump of the electron initiates a betatron and a synchrotron oscillation. These oscillations are damped with a characteristic time (10^{-2}-10^{-3} sec) that is much lower than the polarization time of the Sokolov-Ternov effect (10^{+2}-10^{+3} sec). One can neglect the latter during the time of the oscillation initiated by one photon emission. We are left with only the bending of the spin away from the closed solution **n**. It is caused by the perturbing field **b**(s) associated

with the oscillations. We have seen in Section 5. that the bending becomes significant near a spin resonance.

In an ideally planar ring and at high energy there is no vertical betatron and synchrotron oscillations as the vertical dispersion vanishes (one neglects here the small vertical angle of the electron recoil at photon emission). The perturbing field **b**(s) due to horizontal betatron and synchrotron oscillations is vertical and does not bend the spin, aligned along the vertical closed solution **n**. The ring is perfectly spin-transparent. That situation is different from a proton beam that has a finite vertical emittance and that may be depolarized when crossing an intrinsic resonance even if there is no defects (see Section 7.). Therefore, in electron storage rings the depolarization is mainly due to defects that drive spin resonances of all kinds.

After one photon emission the generated perturbing field **b**(s) decreases in amplitude as the betatron and synchrotron oscillations. The bending away from **n** also decreases and after complete damping the spiraling motion, in the vicinity of a spin resonance, becomes a precession about **n** with a finite opening angle (see Fig. 15). The final deviation of the spin vector **S** from its initial state, assumed parallel to **n**, is a vector **d**, proportional to the energy jump, that precesses with a phase determined by the time of the photon emission. Quite generally the motion of the electrons is linear and the emitted photons are uncorrelated. The deviation vectors **d** of successive photon emissions add up incoherently. They have different amplitudes and phases. As the time of photon emission and the energy jump are random, the spin motion becomes a random process, i.e. a spin diffusion away from the spin closed solution **n**. Here again the spin behavior of polarized electrons and protons are different. The spin motion of a proton is deterministic and beam depolarization results from the incoherent spread of trajectories and energies. For an electron the spin motion is random and beam depolarization results from the random quantum fluctuations of synchrotron radiation. Moreover, the electron beam depolarization is an irreversible process. On the contrary proton beam polarization can be restored. A Siberian Snake is an example of polarization restore after one turn. That also explains why Siberian Snakes are not efficient to overcome depolarization in electron rings[49].

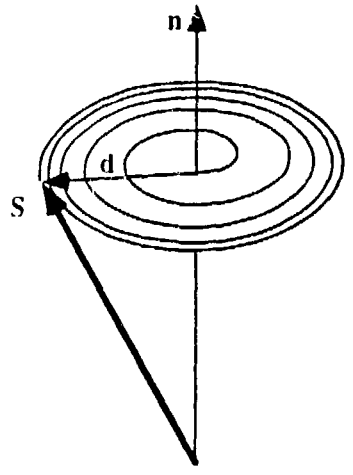

Figure 15: On a spin resonance the spiraling motion of a spin vector **S** excited by the an isolated photon emission. After oscillation damping the deviation from **n** is the vector **d** that precesses about **n**.

In units of the relative energy jump $\delta E/E$, the deviation vector **d** is usually named the spin-orbit coupling vector (here one avoids to use the frequent notation $\gamma\partial\mathbf{n}/\partial\gamma$, that refers to calculations of Ya. Derbenev and A. Kondratenko[50], where the vector **n** is not the spin closed solution[51]). It depends on the longitudinal coordinate s of the electron at the time of the photon emission. It receives contributions from the horizontal and vertical (x and z) betatron oscillations as well as from the synchrotron (s) oscillation. In the linear approximation of the orbital motion these contributions just linearly add up. Each contribution can be expressed as an integral over s of the coupling between the spin motion and the considered orbital oscillation. These integrals are named the spin-orbit coupling integrals $J_{x,z,s}(s)$. The ring becomes spin-transparent when these integrals vanish, making **d** vanishing too.

For a single energy jump the decrease of the polarization P along the spin closed solution **n** is given by:

$$\delta P = \frac{1}{2}\left|\mathbf{d}\,\frac{\delta E}{E}\right|^2 \tag{25}$$

Within the linear approximation the rate of the polarization decrease is obtained by summing the effects of all the successive energy jumps per unit time. Averaging over the coordinate s and the energy jump δE, one obtains:

$$\frac{1}{P}\frac{dP}{dt} = \frac{1}{2}\dot{N}\left\langle\left|\mathbf{d}\,\frac{\delta E}{E}\right|^2\right\rangle \tag{26}$$

where $\dot{N}$ is the photon emission rate and the brackets < > indicate the averaging. It gives the depolarization time τ_d that can also be expressed in terms of the Sokolov-Ternov polarization time τ_p:

$$\frac{\tau_p}{\tau_d} = \frac{11}{18} \langle |\mathbf{d}|^2 \rangle \tag{27}$$

That simple model of the depolarization process by resonant spin diffusion leads to a rough estimate of the equilibrium polarization P_{eq}:

$$P_{eq} \approx \frac{8}{5\sqrt{3}} \frac{1}{1 + \tau_p / \tau_d} \tag{28}$$

Ya. Derbenev and A. Kondratenko[50] have derived a more elaborate formula giving the equilibrium polarization for an arbitrary configuration of magnetic field:

$$P_{eq} = \frac{8}{5\sqrt{3}} \frac{\langle \left|\rho^{-3}\right| \mathbf{b}.(\mathbf{n} - \mathbf{d}) \rangle}{\langle \left|\rho^{-3}\right| \left(1 - \frac{2}{9}(\beta.\mathbf{n})^2 + \frac{11}{18} |\mathbf{d}|^2\right) \rangle} \tag{29}$$

where ρ is the bending radius, $\mathbf{b}$ a unit vector along the transverse component of the field and β a unit vector along the reference orbit. The formula reproduces the maximum 92.4% polarization for an ideally planar without imperfections where the spin-orbit coupling vector $\mathbf{d}$ and $\beta.\mathbf{n}$ vanish. The $\mathbf{d}$-linear term in the numerator of that formula usually gives a negligible contribution as compared to the quadratic term in the denominator. The contributions of the electron recoil during photon emission, that have also been included in other calculations[52, 53], appear to be negligible at high energy.

The effective polarization rate is the sum of the Sokolov-Ternov rate τ_p^{-1} and of the depolarization rate τ_d^{-1}. Therefore the polarization time τ is lower than the ideal value τ_p in presence of imperfections. When the polarization time is too long to reach the equilibrium polarization, one can derive its value P_{eq} just by measuring the rate of increase of the polarization at the beginning and by using the Formula 28. It can also be used to calibrate in polarization degree the experimental data of a polarimeter (see Fig. 16).

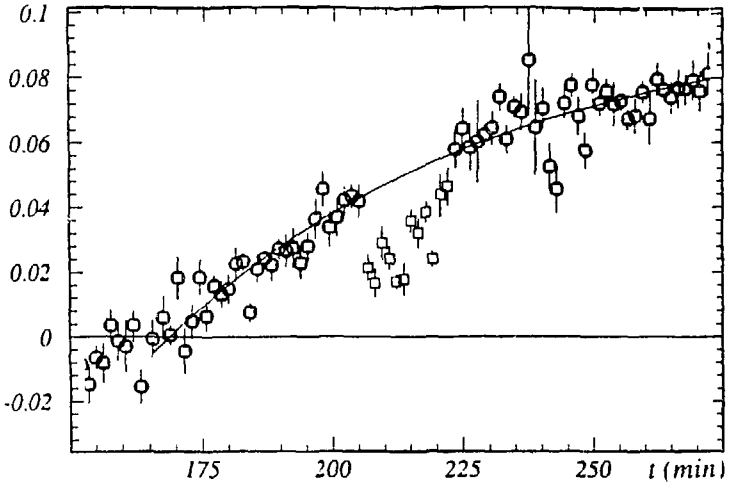

Figure 16: Polarimeter data versus time t at an energy of 46.55 GeV in LEP[46]. The fitted polarization time is 64 min leading to an equilibrium polarization of 20%.

If one knows the defects, the spin-orbit coupling vector can be calculated and numerical codes, for instance SLIM[54], have been developed to calculate it and to estimate the equilibrium polarization. Most of these codes assume that the betatron and synchrotron oscillations are linear and use a matrix formalism. They extend the codes that calculate the orbital motion to the calculation of the spin motion.

As the spin precession scales linearly with energy when a ring is ramped in energy (see Formula 11), the spin-orbit coupling vector also increases linearly with energy. The spin resonances become more and more strong and eventually overlap. The Figure 17 shows a detailed scan of polarization as function of beam energy at the SPEAR storage ring[39]. It shows the depolarization on many spin resonances in a small energy interval, particularly near the synchrotron resonance $\gamma a = 8$ at 3.5 GeV. Moreover several non-linear spin resonances appear harmful, particularly synchrotron satellites of the horizontal betatron resonance $\gamma a = 3 + Q_x$. Some analytical calculations[55] have been done and some numerical codes[56, 57] have also been developed to estimate non-linear depolarization effects that are expected to become important at high energies.

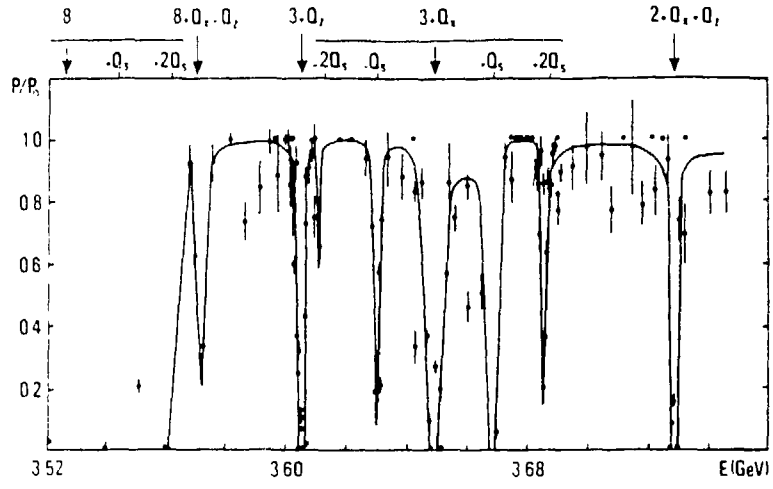

Figure 17: Relative polarization P/P_0 ($P_0 = 92.4\%$) versus beam energy at SPEAR[39]. The solid line is a hand-drawn line to guide the eye. The spin resonances labelled :$k + k_x Q_x + k_z Q_z + k_s Q_s$ are indicated above the figure.

The optimum equilibrium polarization is obtained for a particular choice of the beam energy. It corresponds to a spin tune with an integer part far from multiples of the ring superperiodicity to avoid strong systematics defects and far from the betatron tunes to avoid contribution of large harmonics of the perturbed closed orbit. The fractional part is also set equal to 1/2, i.e. the largest distance from the strong synchrotron resonances. However, at high energies the optimum polarization becomes lower than the maximum allowed by the Sokolov-Ternov effect (see Table 1.) due to the increase with energy of the spin-orbit coupling vector.

In the high-energy storage rings it becomes necessary to improve the equilibrium polarization by the spin-matching, i.e. the corrections to make the ring more spin-transparent. The first step is to correct the vertical closed orbit and the vertical dispersion using dipole correctors and conventional algorithms. Doing so one minimizes the deviation of the spin closed solution **n** from the vertical and one minimizes the beam vertical emittance. The ring is made more spin-transparent. The second step is to use special algorithms to compensate the nearby spin resonances, particularly the nearest and strongest synchrotron resonances. One excites harmonics of the closed orbit distortion that are close to the spin tune and that drive these resonances. These harmonics do not affect the closed orbit in a visible way as they are far from the betatron tunes, but they greatly act upon the equilibrium polarization. The latter procedure, named harmonic spin-matching, has been successfully applied at PETRA[58] and TRISTAN[45].

11. Energy calibration by depolarization on an artificial RF spin resonance

The first application of beam polarization in an electron storage ring is its accurate calibration in energy. That has been applied in several rings: VEPP2-M[59], BESSY[38],VEPP4[60], DORIS II[61], CESR[42] and LEP[46]. The method used is based on a RF resonance technique. It can be done even with a modest degree of polarization. The principle is similar to a NMR experiment, although the magnetic energy absorbed by the beam is too small to be directly measured as in NMR experiments.

At LEP the RF resonance technique has been applied at 46.5 GeV corresponding to a spin tune of 105.5. After one-hour waiting time, when the polarization reaches about 10%, a small radial RF magnetic field, produced by a kicker, is turned on. The applied field excites a RF spin resonance. The tune value of that resonance is varied by changing the frequency of the RF field. When the scanned range of tune overlaps the spin tune of the beam, the RF resonance is crossed, and the beam is depolarized (see Fig. 18). To determine the RF frequency at which depolarization occurs the central frequency is varied and the polarization is continuously monitored with the polarimeter. From that measurement the spin tune and the energy of the beam are deduced. On the contrary of a proton beam accelerated in a synchrotron, the spin tune of the beam is fixed and the tune of the RF spin resonance is varied.

The RF magnetic field has a very small integral value, about 4 Gm only. For the spin motion that radial field is a perturbing field that can be analyzed in frequency to find the spin resonances that it excites, as explained in Section 5. The tunes of these RF resonances are given by:

$$\nu = n \pm \frac{f_{RF}}{f_{rev}} \tag{30}$$

where f_{RF}, f_{rev} are the applied RF and revolution frequencies respectively and n is any integer. The frequency span is typically 112 Hz per minute corresponding to a spin tune range of 0.01 and an energy range of 4.4 MeV. The beam energy E is deduced from the frequency f_{RF} at which depolarization is observed:

$$E = \frac{m_0 c^2}{a}\left(n \pm \frac{f_{RF}}{f_{rev}}\right) \tag{31}$$

after lifting the sign ambiguity (obtained by observing the change of the depolarization frequency when the energy is varied). The limit in accuracy of this calibration method can be as small as 10^{-5}.

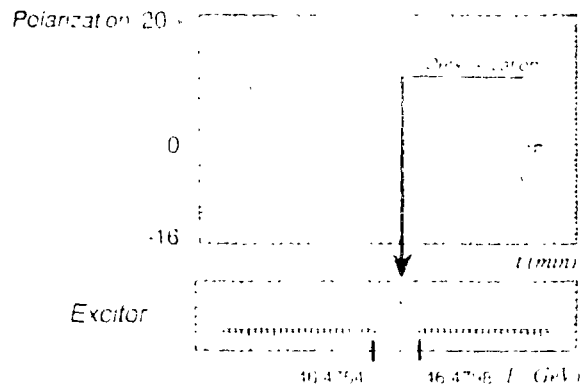

Figure 18: The polarization versus the time t in a calibration experiment at LEP. Depolarization is observed when the RF field (excitor) is turned on with a frequency span corresponding to an energy range (4.4 MeV) overlapping the beam energy E.

The accurate energy calibration has been used to measure the mass of the K mesons[62,63], ϕ meson[64], ψ meson[65] and of the Υ, Υ', Υ'' mesons[10,12,61,66,67]. One must also mention the very accurate comparison[68] of the gyromagnetic anomaly of electrons and positrons at VEPP2-M by again a RF technique similar to an NMR experiment showing that the sophisticated spin manipulations in Nuclear Magnetic Resonance can also be used in electron storage rings.

12. Polarized beams for electron-positron and electron-proton experiments.

In a storage ring collider the Sokolov Ternov effect allows the electron and positron beams to become transversely polarized in opposite directions. That polarization scheme has been used in a few experiments on e^+e^- collisions. At SPEAR[69] the angular distribution for the reactions e^+-$e^- \rightarrow e^+$-e^- and e^+-$e^- \rightarrow \mu^+\mu^-$ has been studied at different energies up to 3.7 GeV. The azimuthal asymmetry of e^+e^- confirmed the high degree of polarization for both beams in the collision mode and at high luminosity. The angular distribution of μ^+-μ^- was found to be in good agreement with the predictions of quantum electrodynamics at these medium energies. In another experiment at SPEAR[70] the annihilation e^+-$e^- \rightarrow$ multi-hadrons has been studied at 7.4 GeV center of mass energy. The angular distribution of the final state particles was found consistent with the quark parton model, in particular the polarization data confirmed that quarks are spin 1/2 particles. At VEPP 2M experiments with polarized beams in collision mode have also been performed to study the production of μ^+-μ^- pairs[71] at 2.65 GeV center of mass energy and of K^+K^- pairs[72] at the ϕ meson energy (510 MeV).

Nowadays, the interest of polarized electron beams at high energies has come up again to test the Standard Model of the electro weak interaction. These tests require a longitudinal polarization at the collision points, i.e. a polarization vector pointing to the beam direction. The

transverse polarization, built up in the bending magnets of the storage ring arcs by the synchrotron radiation, must be rotated by 90° at the collision points. The spin closed solution **n**, that is vertical in the arcs, is first bent into the beam direction by a 90° spin rotator before the collision point. Then a second rotator bends it back to the vertical direction after the collision point. These two rotators are two sets of bending magnets with an antisymmetric configuration w.r.t. the collision point in the vertical plane. The antisymmetry has the advantage to leave the closed orbit unperturbed in the arcs. The simplest configuration[72] of rotators is an S-bend, made of four vertically bending magnets (see Fig. 19). It produces a vertical orbit bump around the collision point, where the orbit crosses the median plane at a vertical angle α. Since the spin rotation angle is γa larger than the bending angle (see Formula 11.), the 90° rotation required to align the spin vector along the orbit results from the inclination of the latter by $\alpha = \pi/(2\gamma a)$. In the example of the S-bend rotators proposed[73] for LEP at 46 GeV, the vertical orbit slope is α = 15 mrad.

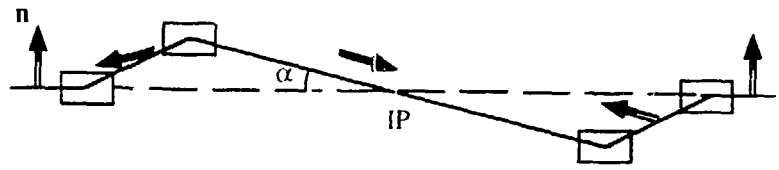

Figure 19: Schematic side view of an S-bend configuration of two spin rotators antisymmetric w.r.t. the collision point IP. Each rotator consists of two magnets vertically bending the electron trajectory by an angle α and -2α respectively . With $\alpha = \pi/(2\gamma a)$ the spin closed solution **n** is longitudinal at the IP.

The slope α decreases when the energy increases. It illustrates the first drawback of rotators: the field in the rotator magnets is fixed to obtain the right spin rotation w.r.t. the orbit and the orbit bump varies with the electron energy, according to the Formulae 11. and 13. Moreover, to change the sign of the electron helicity at the collision point, i.e. to invert the longitudinal polarization, one has to change the sign of the fields in the rotator magnets. But the orbit bump is also inverted and one is often obliged to move the magnets. Special masks must also be installed to protect the detector of the experiment against the synchrotron radiation emitted in the rotator magnets. A second drawback results from the direction of the spin closed solution **n** that is no more parallel to the magnetic field in the rotator magnets. In the latter the Sokolov-Ternov tends to polarize the beams along the field direction different from **n**. The result is an ultimate polarization degree lower than the maximum 92.4%. The reduction is quantitatively given by the Formula 29. in which the scalar product **b.n** becomes lower than one in the rotator magnets. The polarization decrease can only be minimized by an optimization of the rotator magnet configuration, in particular by using long magnets with low fields. The last drawback is the breakdown of the spin-transparency as **n** is also no more vertical. One can consider the rotators as very large defects. The spin-orbit coupling integrals $J_{x,z,s}$ and the spin-orbit coupling vector **d** do not vanish all along the ring circumference. The depolarization by spin

diffusion is large and the equilibrium polarization low. However, on the contrary of the ring imperfections, these defects are known and in principle one can adjust the ring optics and the rotator magnets to cancel out the integrals $J_{x,z,s}$. That procedure is the spin-matching of the rotators[74]. Finally, there are different possibilities of rotators depending on the configurations and the optics of the ring interaction regions. For HERA the so-called mini-rotators[75], that are sandwiches of horizontally and vertically bending magnets, have been designed and built to match the separation of the electron and proton beams on both sides of the interaction point where they collide head-on.

Experiments with polarized beams can only be considered if the time to wait for the polarization after beam injection and storage is reasonable. The polarization time τ_p must be short. The five hours polarization time of LEP at 46 GeV needs to be reduced. It can be achieved by installing wiggler magnets with high fields and small bending radius ρ. The third power dependence of τ_p on ρ allows a substantial gain. Asymmetric wigglers[76], made of three magnets with a high-field central one compensated by the low-field side ones, have been installed at LEP. They would reduce the polarization time below one hour at 46 GeV. However, it is expected that they will also affect the equilibrium polarization. On one hand, installing them in a dispersion-free region of the ring, they do not generate betatron oscillations. The average of the spin-orbit coupling vector **d** is reduced. According to the Formulae 26. and 27., the ratio τ_p/τ_d is also reduced and the equilibrium polarization is increased[76]. On the other hand, they generate synchrotron oscillations that increase the beam energy spread. These oscillations in energy induce a modulation of the spin tune (see Formula 14.) that drive synchrotron satellites of all the spin resonances. A large enhancement of depolarization due to these satellites is expected[55].

Finally, the last, but not the least, requirement for polarized beam experiments at electron storage rings is both high degree of polarization and high luminosity. At high energy one needs an efficient spin matching to compensate the depolarization effects of ring imperfections and to achieve polarization of at least 50%. Finally, the polarization must be maintained in the collision mode at high luminosity. Although that was realized in the e^+-e^- experiments at SPEAR and VEPP-2M, there was an experimental indication[43] at PETRA that at higher energy the beam-beam interaction can reduce the equilibrium polarization.

13. References

1. T. Aniel et al., *Journal de Physique*, **46** (1985) 499.
2. P. A. Chamouard et al, *Journal de Physique*, **51** (1990) 569.
3. F. Z. Khiari et al., *Phys. Rev. D*, **39** (1989) 45.
4. W. Brefeld et al, *Nucl. Instr. Meth.*, **228** (1985) 228.
5. C. Y. Prescott et al., *Phys. Lett.*, **77B** (1978) 347.
6. C. Y. Prescott, private communication.
7. L. Knudsen et al, *Phys. Lett.*, **270B** (1991) 97.
8. B. W. Montague, *Physics Reports*, **113** (1984) 2.
9. J. Buon, *CAS Proc.*, CERN reports **87-03** (1987) 647 and **89-01** (1989) 93.
10. Ya. S. Derbenev and A. M. Kondratenko, *Sov. Phys.-Dokl.*, **20** (1976) 562.
11. Ya. S. Derbenev et al, *Part. Acc.*, **8** (1978) 115.
12. A. D. Krisch, *Phys. Rev. Lett.*,**63** (1989) 1137.
13. J. E. Goodwin, *Phys. Rev. Lett.*,**64** (1990) 2779.
14. E. D. Courant and R. D. Ruth, *BNL Report*, **51270** (1980).
15. R. D. Ruth, *IEEE Trans. Nucl. Science*, **30** (1983) 286.
16. A. Tkatchenko, *1990 EPAC Conf.*, ed. P. Marin and P. Mandrillon (Nice,1990) p. 159.
17. A. W. Chao, *AIP Conf. Proc.*, **87** (1981) 395.
18. A. W. Chao, *IEEE Trans. Nucl. Science*, **30** (1983) 2383.
19. D. P. Barber, *1990 EPAC Conf.*, Ed. P. Marin and P. Mandrillon (Nice,1990) p. 164.
20. A.A. Sokolov and I.M.Ternov, *Sov. Phys.-Doklady*, **8** (1964) 1203.
21. J. S. Bell, *CERN report*, **75-11** (1975).
22. Particle Data Group, J. J. Hernandez et al., *Phys. Lett. B*, **239** (1990).
23. CODATA Recommended values, *Journ. of Research of NBS*, **92** (1987) 85.
24. V.Bargmann, L.Michel, V.L.Telegdi, *Phys. Rev. Lett.* **2** (1959) 435.
25. L. T. Thomas, *Phil. Mag.* **3** (1927) 1.
26. J.D.Jackson, *Classical Electrodynamics* (J. Wiley and sons,2nd ed.,1975) p.541.
27. Ya. S. Derbenev et al, *Sov. Phys.-Doklady*, **15** (1970) 583.
28. K. Steffen, *DESY HERA report*, **82/02** (1982).
29. N. Horikawa, in *Proc. 9th Int. Symp. on High Energy Spin Physics*, ed. K.-H. Althoff and W. Meyer (Springer-Verlag, 1991) p. 172.
30. T. Khoe et al, *Part. Accel.*, **6** (1975) 213.
31. M. Froissart and R. Stora, *Nucl. Instr. Meth.*, **7** (1960) 297.
32. P. A. Chamouard, private communication.
33. Ya. S. Derbenev and A. M. Kondratenko, *Novosibirsk preprint*, **78-74** (1978).
34. V. N. Baier, *Sov. Phys.-USPEKHI*, **14** (1976) 1063.
35. S. I. Serednyakov, *Sov. Phys.-JETP*, **44** (1972) 695.

36. R. Belbéoch et al, in *Proc. USSR Nat. Conf. Particle Accelerators* (1968) p.129.
37. The Orsay Storage Ring Group, in *Proc. 8th Int. High Energy Accelerators* (CERN, Geneva, 1971) p. 127.
38. K. Ott, private communication and BESSY Annual Report 1988.
39. J. R. Johnson et al, *Nucl. Instr. Meth.*, **204** (1983) 261.
40. A. S. Artamonov et al, *Phys. Lett.*, **118B** (1982) 225.
41. D. P. Barber, *DESY report*, **M-83-29** (1983).
42. W. Mackay et al, *Phys. Rev.*, **29** (1984) 2483.
43. H. D. Bremer et al, *DESY report*, **M-82-26** (1982).
44. D. P. Barber, private communication.
45. K. Nakajima et al, Paper TUS04A at the *1992 EPAC Conf.* (Berlin 1992).
46. L. Arnaudon et al, *CERN report*, **SL/92-16** (1992), to be published in Phys. Lett. B (1992).
47. J. D. Jackson, *Rev. Mod. Phys.*, 48 (1976) 417.
48. J. S. Bell and J. M. Leinaas, *Nucl. Phys. B*, **284** (1987) 488.
49. J. Buon, *LAL/RT report*, **84-05** (1984).
50. Ya. S. Derbenev and A. M. Kondratenko, *Sov. Phys.-JETP*, **37** (1973) 968.
51. K. Yokoya, *DESY report*, **86-057** (1986).
52. L. N. Hand and A. Skuja, *Phys. Rev. Lett.*, **59** (1987) 1910.
53. D. P. Barber and S. R. Mane, *Phys. Rev. A*, **37** (1988) 456.
54. A. W. Chao, *Nucl. Instr. Meth.*, **180** (1981) 29.
55. J. Buon, *Part. Acc.*, **32** (1990) 153.
56. S. R. Mane, *Fermilab report*, **FN-466** (1987).
57. J. Kewisch, *DESY report*, **83-032** (1983).
58. H. D. Bremer et al, *DESY report*, **82-026** (1982).
59. Ya. S. Derbenev et al, *Part Acc* , **10** (1980) 177.
60. A. E. Bondar et al, in *Proc. 12th Int. Conf. on High Energy Accelerators*, ed. T. Cole and R. Donaldson (Fermilab 1983) p. 240.
61. D. P. Barber et al, *Phys. Lett* , **135B** (1984) 498.
62. L. M. Barkov et al, *Nucl Phys.*, **B148** (1979) 53.
63. L. M. Barkov et al, *Novosibirsk preprint*, **83-85** (1983).
64. A. D. Bukin et al, *Yad. Fiz.*, **27** (1978) 976.
65. A. A. Zholents et al, *Phys. Lett.*, **96B** (1980) 214.
66. A. S. Artamonov et al, *Phys. Lett.*, **137B** (1984) 272.
67. S. E. Baru et al, *Z. Phys. C*, **30** (1986) 551.
68. I. B. Vasserman et al, *Phys. Lett.*, **198** (1987) 302.
69. J. G. Learned et al, *Phys. Rev. Lett.*, **35** (1975) 1688.
70. R. F. Schwitters et al, *Phys. Rev. Lett.*, **35** (1975) 1320.
71. L. M. Kurdadze et al, *Novosibirsk preprint*, **75-66** (1975).
72. V. N. Baier, *Sov. Phys.-USPEKHI*, **14** (1972) 695.
73. H. Grote et al, *1990 EPAC Conf.*, Ed. P. Marin and P. Mandrillon (Nice,1990) p. 1497.
74. J. Buon, *Nucl. Instr. Meth* , **A 275** (1989) 226.

75. J. Buon and K. Steffen, *Nucl. Instr. Meth.*, **A 245** (1986) 248.
76. A. Blondel and J. M. Jowett, *LEP note* **606** (1988).